SUPPLEMENTARY INFORMATION

Wide-Range Ideal 2D Rashba Electron Gas with Large Spin Splitting in Bi_2Se_3/$MoTe_2$ Heterostructure

Te-Hsien Wang and Horng-Tay Jeng*

Department of Physics, National Tsing Hua University, Hsinchu 30013, Taiwan

E-mail: jeng@phys.nthu.edu.tw

Table of contents:

*To whom correspondence should be addressed

I. Substrate Effect

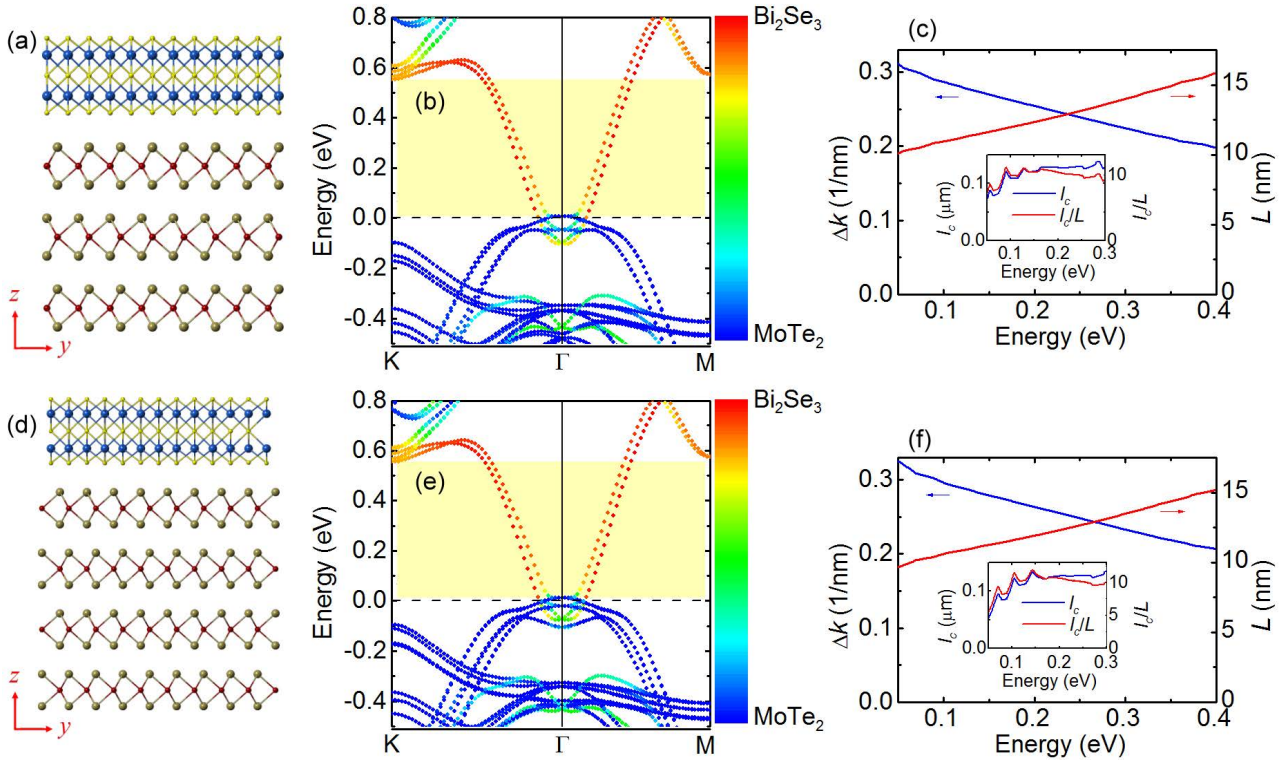

Figure S1: (a) Side view of the 1QL-Bi_2Se_3/3TL-$MoTe_2$ heterostructure. (b) Electronic band structure of the 1QL-Bi_2Se_3/3TL-$MoTe_2$ heterostructure, where the Bi_2Se_3 and the $MoTe_2$ components are represented by the color of the dots. The yellow-shaded region indicates the energy region in which, except for the RB states, there is no other electronic states. (c) The WND between the two RBs Δk of the 1QL-Bi_2Se_3/3TL-$MoTe_2$ heterostructure and the corresponding spin precession length L as functions of energy. The inset shows the coherence length l_c and the ratio of the l_c to the spin precession length as functions of energy. (d-f) are the counterparts of (a-c), respectively, for the case of the 1QL-Bi_2Se_3/4TL-$MoTe_2$ heterostructure.

Figures S1b and S1e, respectively, show the electronic structures of the 1QL-Bi_2Se_3/3TL-$MoTe_2$ and the 1QL-Bi_2Se_3/4TL-$MoTe_2$ heterostructures, in which, as shown in Figures S1a and S1d, the $MoTe_2$ TLs are stacked in the $2H$ sequence. The widths of the energy window within which only the RB states exist (the yellow-shaded region) for the cases of 1QL-Bi_2Se_3/3TL-$MoTe_2$ and 1QL-Bi_2Se_3/4TL-$MoTe_2$ are both 0.54 eV and nearly the same as that of the case 1QL-Bi_2Se_3/2TL-$MoTe_2$ heterostructure 0.53 eV. The WND between the two RBs, the spin precession length L, and the coherence length l_c are also almost not changed by the increase of the

substrate ($MoTe_2$) thickness for the cases of 1QL-Bi_2Se_3/nTL-$MoTe_2$ ($n \geq 2$) heterostructures as shown in Figures S1c, S1f, and Figure 5f of the main text.

II. Strain Effect

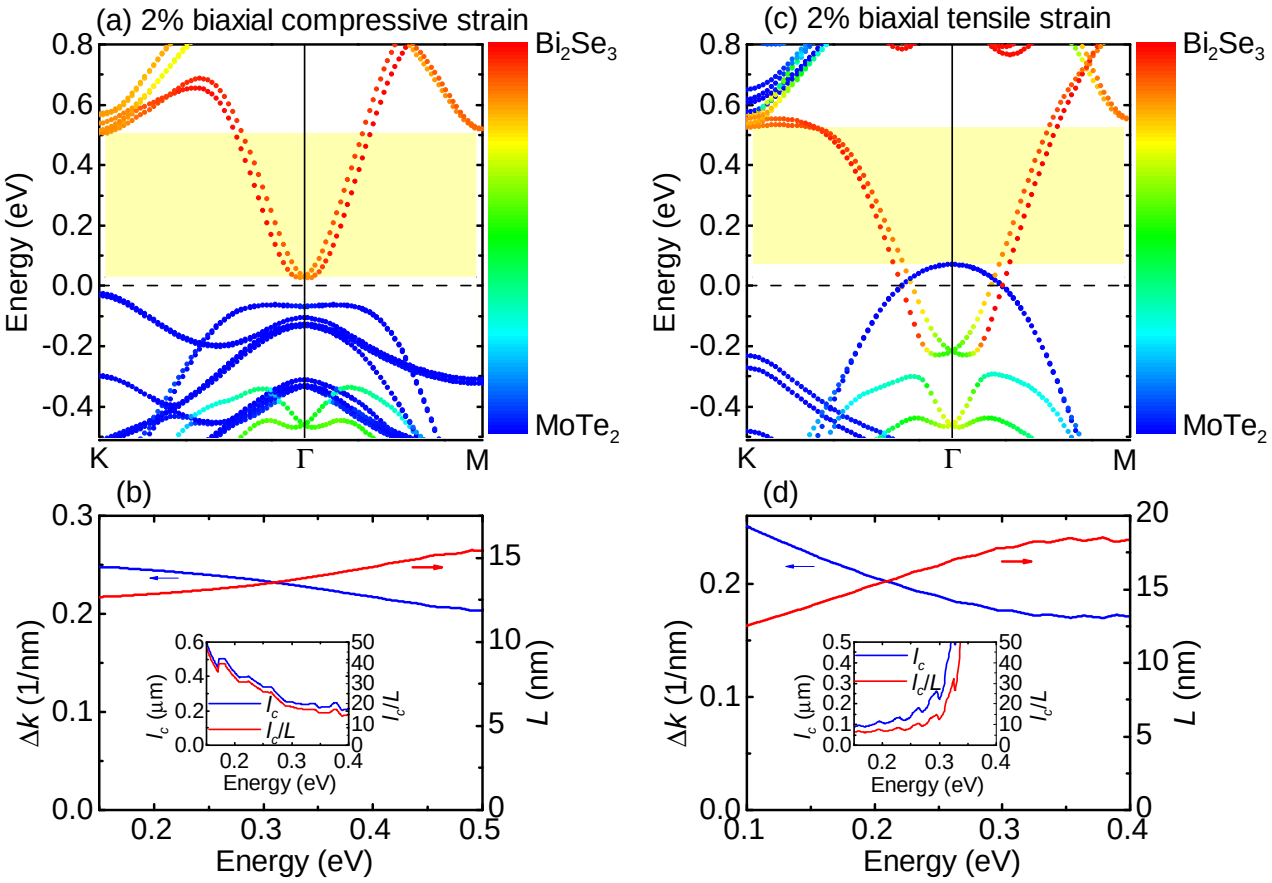

Figure S2: (a,c) Electronic band structure of the strained 1QL-Bi_2Se_3/2TL-$MoTe_2$ heterostructure, where the Bi_2Se_3 and the $MoTe_2$ components are represented by the color of the dots. The yellow-shaded region indicates the energy region in which, except for the RB states, there is no other electronic states. (b,d) The WND between the two RBs Δk of the strained 1QL-Bi_2Se_3/2TL-$MoTe_2$ heterostructure and the corresponding spin precession length L as functions of energy. The inset shows the coherence length l_c and the ratio of the l_c to the spin precession length as functions of energy. (a,b) are for the case that a 2% biaxial compressive strain is applied. (c,d) are for the case that a 2% biaxial tensile strain is applied.

Because increasing the thickness of the $MoTe_2$ layer do not cause significant changes of the RBs for the cases of the 1QL-Bi_2Se_3/nTL-$MoTe_2$ ($n \geq 2$) heterostructures, we, as an example,

consider the case of 1QL-Bi_2Se_3/2TL-$MoTe_2$ heterostructure. Figure S2a (S2c) shows the electronic structure of 1QL-Bi_2Se_3/2TL-$MoTe_2$ under a 2% biaxial compressive (tensile) strain. As can be seen, the presence of a 2% biaxial compressive strain separates the Bi_2Se_3 RBs from the $MoTe_2$ bands and causes an energy gap of 51.2 meV. The coherence length l_c and the ratio of the l_c to the spin precession length L are generally at least two times larger than those of unstrained counterpart as shown in the insets of Figure 2Sb and in Figure 5f of the main text. On the other hand, in the presence of a 2% biaxial tensile strain, the Γ-point energy of the $MoTe_2$ band at the is higher than that of the RBs. The energy difference is 147 meV, which is slightly higher than that of unstrained counterpart, 123 meV.

III. Electronic structures of 3QL-Bi_2Se_3/1TL-$MoTe_2$ and 2QL-Bi_2Se_3/2TL-$MoTe_2$ heterostructures

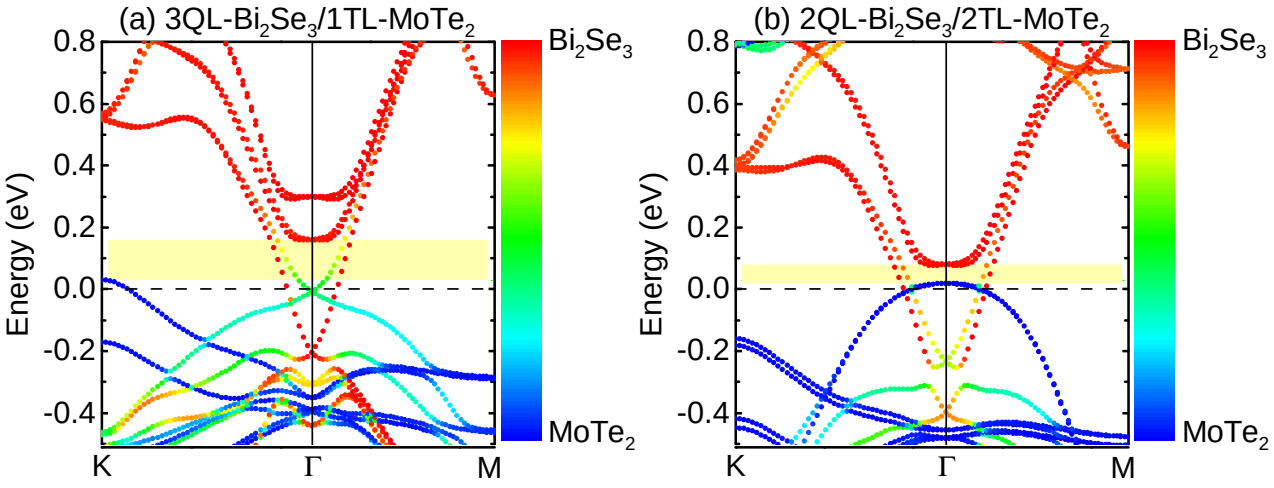

Figure S3: Electronic structures of (a) the 3QL-Bi_2Se_3/1TL-$MoTe_2$ heterostructure and (b) the 2QL-Bi_2Se_3/2TL-$MoTe_2$ heterostructure, where the Bi_2Se_3 and the $MoTe_2$ components are represented by the color of the dots. The yellow-shaded region indicates the energy region in which, except for the RB states, there is no other electronic states.

Figure S3a shows the electronic structure of the 3QL-Bi_2Se_3/1TL-$MoTe_2$ heterostructure. Similar to the case of 2QL-Bi_2Se_3/1TL-$MoTe_2$ heterostructure, there are two Dirac cones corresponding

to two sets of TSSs on the interface side and on the vacuum side of the Bi_2Se_3 film. The higher-energy one, whose Dirac point is at 0 eV, corresponds to the TSSs on the interface side. The other one, whose Dirac point is at -0.2 eV, corresponds to the TSS on the vacuum side. In comparison with the case of 2QL-Bi_2Se_3/1TL-$MoTe_2$ heterostructure (See Figure 5b of the main text) and the case of 2QL-Bi_2Se_3/2TL-$MoTe_2$ heterostructure (Figure S3b), the wave functions of the TSSs on the vacuum side shows less $MoTe_2$ component. This is because the tunneling effect of the TSSs will be reduced by increasing the thickness of Bi_2Se_3 film. For the case 2QL-Bi_2Se_3/2TL-$MoTe_2$ heterostructure, the widths of the energy window within which only the RB states exist is as small as 60 meV, which is restricted by the band edge of the $MoTe_2$ band at the Γ point (19 meV) and that of the QWS (79 meV).

IV. Electronic structures of 1QL- and 6QL-Bi_2Se_3 films.

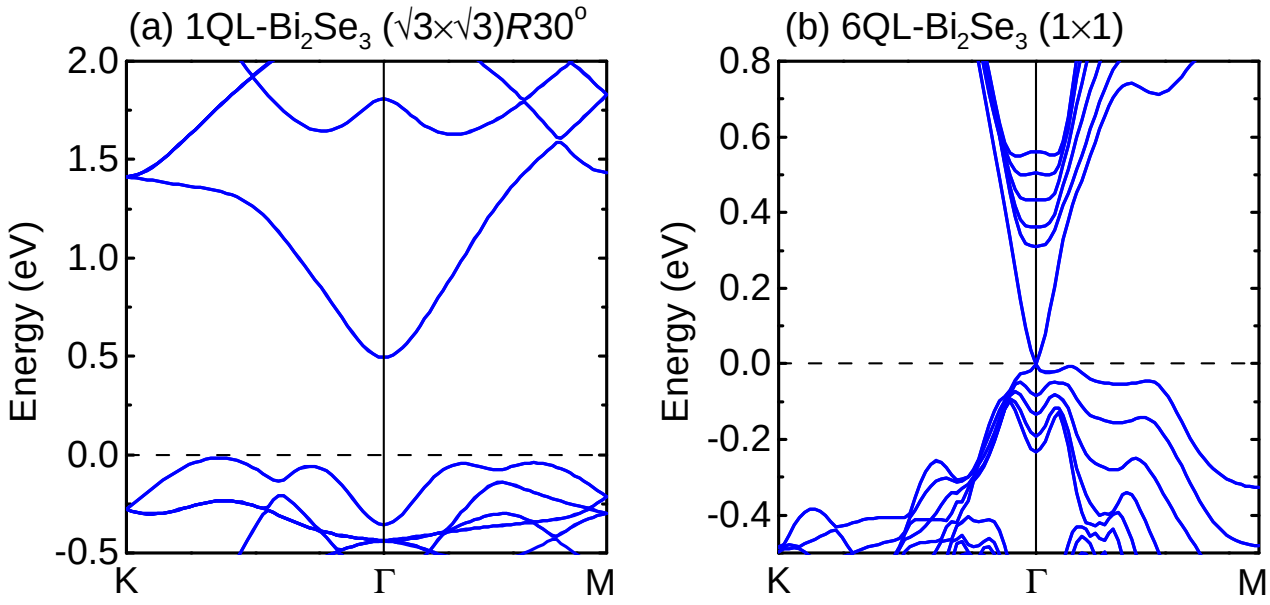

Figure S4: Electronic structures of the free-standing (a) 1QL-Bi_2Se_3 ($\sqrt{3}\times\sqrt{3}$)$R30^\circ$ and (b) 6QL-Bi_2Se_3 (1×1) films.

V. Different interfacial structures

To demonstrate the interface stability as well as the robustness of the Rashba bands, we have studied other interface structures and present one example below. Figure S5a shows the interfacial structure of Fig. 1 of the main text. Only the atomic layers closest to the interface are shown here. Figure S5b shows another interfacial structure with the Bi_2Se_3 layer displaced by a vector of $(\mathbf{T}_1+\mathbf{T}_2)/12$. The relaxed structure is shown in Figure S6. In comparison with the original structure, the changes in the lattice constant and interlayer distance are smaller than one percent. The calculated total energy of this structure is nearly the same as that of the original structure presented in the main text. The energy difference is only 5 meV per supercell with 27 atoms and 156 electrons therein.

Furthermore, the other results such as the electronic bands, the wave number difference and the coherence length, as well as the spin texture and the spin polarization shown in Figure S7, S8, and S9, respectively, are also nearly the same as those of the original structure presented in the main text. Consequently our proposed Rashba bands in the bilayer heterostructure are robust and free from the influence of the interfacial structural changes.

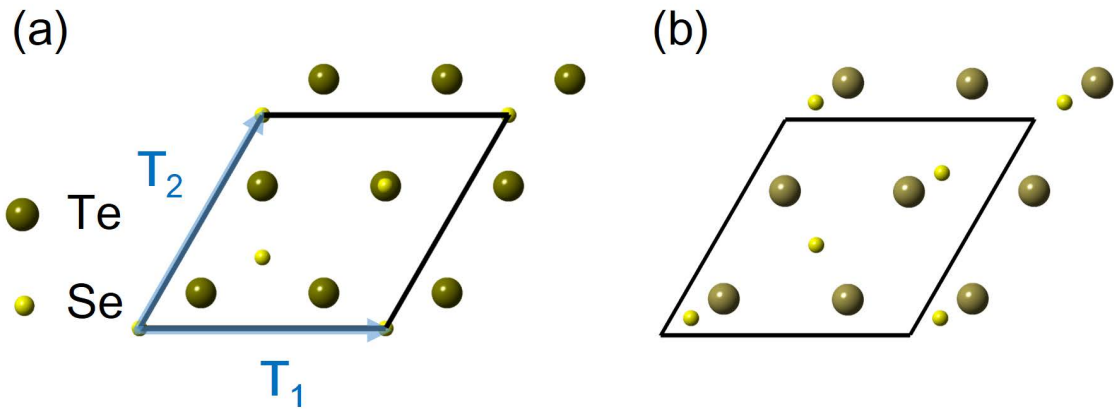

Figure S5: The interfacial structure of the Bi_2Se_3-$(\sqrt{3}\times\sqrt{3})R30^\circ$/$MoTe_2$-$(2\times2)$ heterostructure. (a) The interfacial structure corresponding to the structure shown in Figure 1 of the main text. (b) The interfacial structure with the Bi_2Se_3 layer displaced by a vector of $(\mathbf{T}_1+\mathbf{T}_2)/12$ with respect to (a).

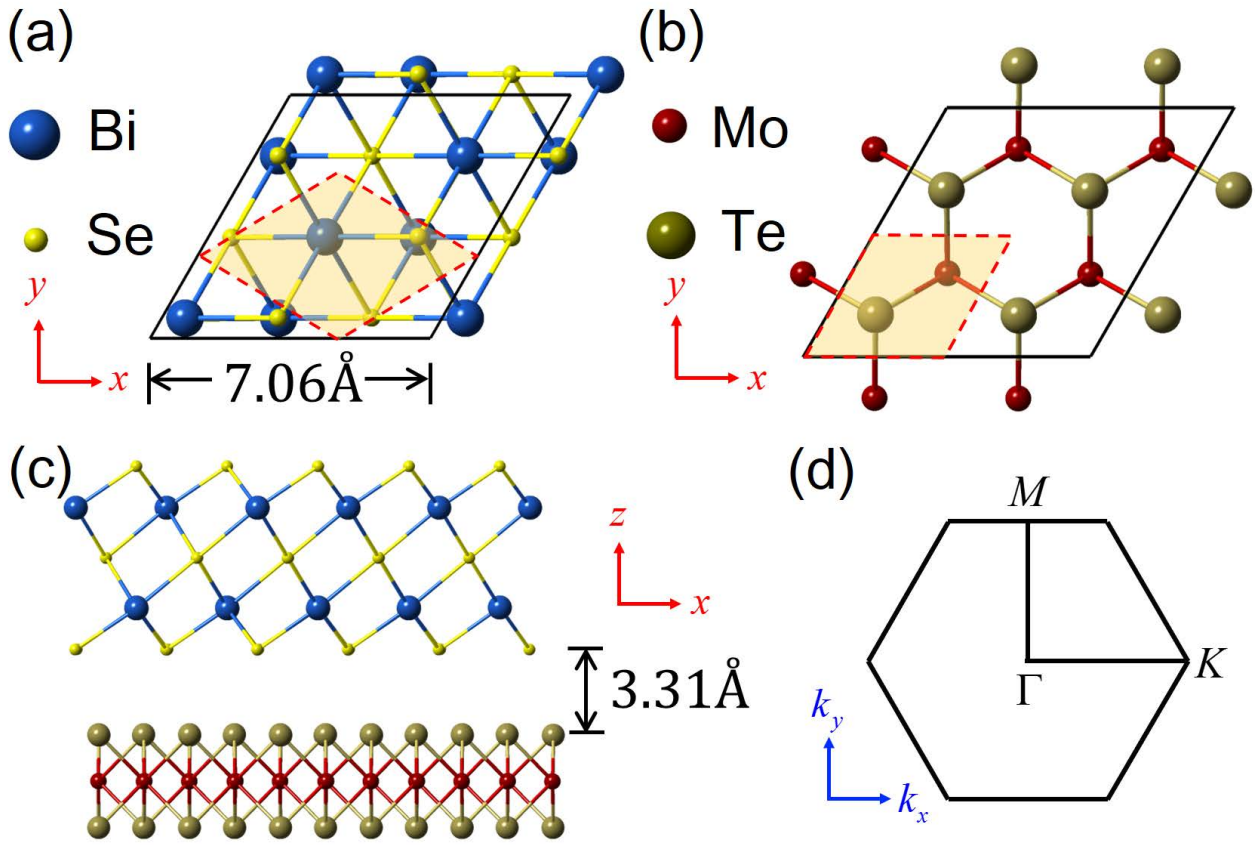

Figure S6: The optimized lattice of the 1QL-Bi_2Se_3/1TL-$MoTe_2$ heterostructure, whose interfacial structure can be seen in Figure S5b. (a) Top view of the Bi_2Se_3 part. (b) Top view of the $MoTe_2$ part. (c) Side view of the whole system. The supercell used in the calculations is denoted in (a) and (b) by the black solid line, in which the Bi_2Se_3-$(\sqrt{3}\times\sqrt{3})R30°$/$MoTe_2$-$(2\times 2)$ system is incorporated. The shaded regions in (a) and (b) denote, respectively, the Bi_2Se_3 and the $MoTe_2$ 1×1 unit cell. The corresponding Brillouin zone is shown in (d).

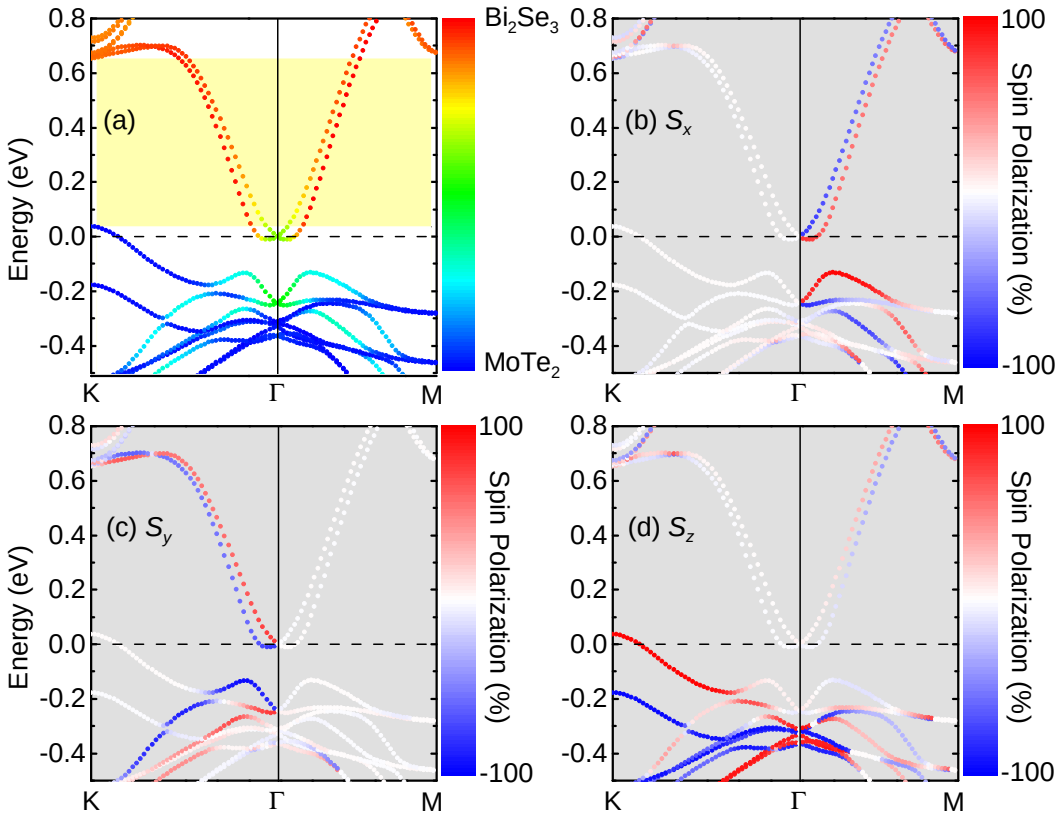

Figure S7: Electronic structures of the 1QL-Bi_2Se_3/1TL-$MoTe_2$ heterostructure shown in Figure S6, where (a) the Bi_2Se_3 and the $MoTe_2$ components, (b-d) spin polarization along the x, y and z directions are represented by the color of the dots. The yellow-shaded region in (a) indicates the energy window (over 0.6 eV) for ideal Rashba bands without any other electronic states.

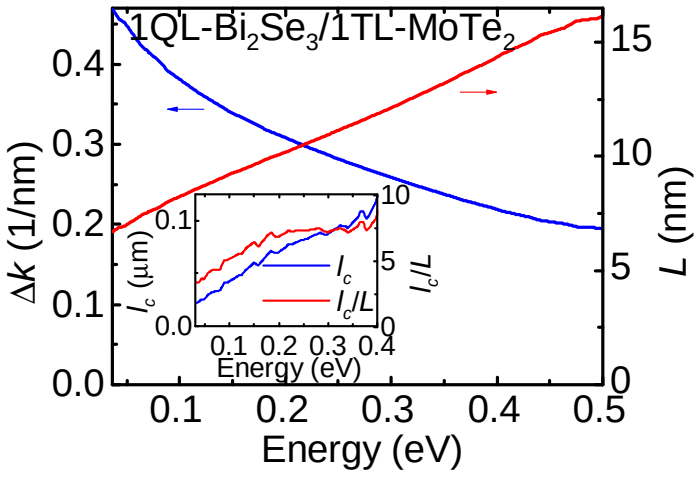

Figure S8: The WND between the two RBs Δk and the corresponding spin precession length L as functions of energy. The inset shows the coherence length l_c and the ratio of the l_c to the spin precession length as functions of energy.

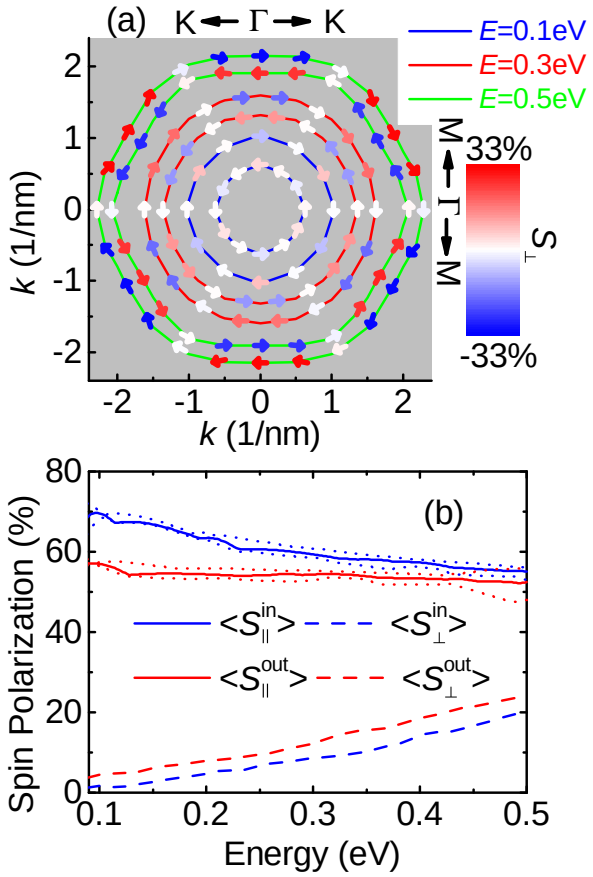

Figure S9: (a) Spin texture of the 1QL-Bi_2Se_3/1TL-$MoTe_2$ heterostructure. The in-plane spin-polarization directions $S_{\parallel}$ are indicated by the arrows. The out-of-plane spin polarizations $S_{\perp}$ are represented by the color of the arrows. (b) The azimuthal average of the magnitude of the spin polarization. The blue (red) lines are those of the inner (outer) Rashba branch, and the solid (dashed) lines are those of the in-plane (out-of-plane) component. The maximum and minimum magnitudes of the in-plane spin polarization are indicated by the dotted lines.

VI. Charge density profiles and overlap integrals of the RBs

In this section we present the charge density profiles and overlap integrals of the RBs to show the difference between the TSS in thick TI (Bi_2Se_3 $\geq$6QL) and our RBs in 1Q Bi_2Se_3, and further demonstrate our Rashba bilayer heterostructure can host the 2D Rashba electron gas.

When the film thickness increases from 1QL to 2QLs, the RB states begin to evolve into the topological surface states. As mentioned in the main text that in the limiting case of an infinite thickness, the wave functions of the top and bottom surface states are completely separated.

Therefore the electron spins do not precess because the spin direction of the electrons on each side of the film aligns along the effective magnetic field. In this case the precession length is meaningless. However, when there is a finite wave-function overlap between the two RB states, the spin do precess during transport. Its precession length is determined by the wave number difference. The decay length of the topological surface states of Bi_2Se_3 is well known larger than 1QL. Thus for the 1QL-Bi_2Se_3, there should not be any electronic state being regarded as a surface state. The wave function overlaps between the two RB states are indeed large. Here we plot the charge density profile of the RB states along the GM direction at energies 0.2, 0.4, and 0.6 eV as shown in Figure S10b-d. Clearly even for the states far away the Gamma point, the wave functions of the two Rashba states do overlap largely with each other.

To have a quantitative understanding, we consider an electron wave, similar to the original approach of Datta-Das (Ref. 1 of the main text), being a linear combination of the two RB states of the same energy propagating along the same direction. The magnitude of the spin polarization perpendicular to the effective magnetic field will be proportional to the wave-function overlap integral of the two RB states. The magnitude of the wave function overlap integral can be estimated from the charge densities obtained from our first-principles calculations. For the wide energy range $0.1\sim0.6$ eV, the calculated overlap integral for the RB states are as high as $0.8\sim0.9$. It is quite close to its maximum possible value, unity. Such a large wave function overlap will cause a large magnitude of the spin polarization perpendicular to the effective magnetic field and hence a good capability of the spin transistor to modulate the spin current. Whereas at the low energy region (about smaller than 0.04 eV), there are some other states (the MoTe2 band) contaminating the transport properties as mentioned in the main text.

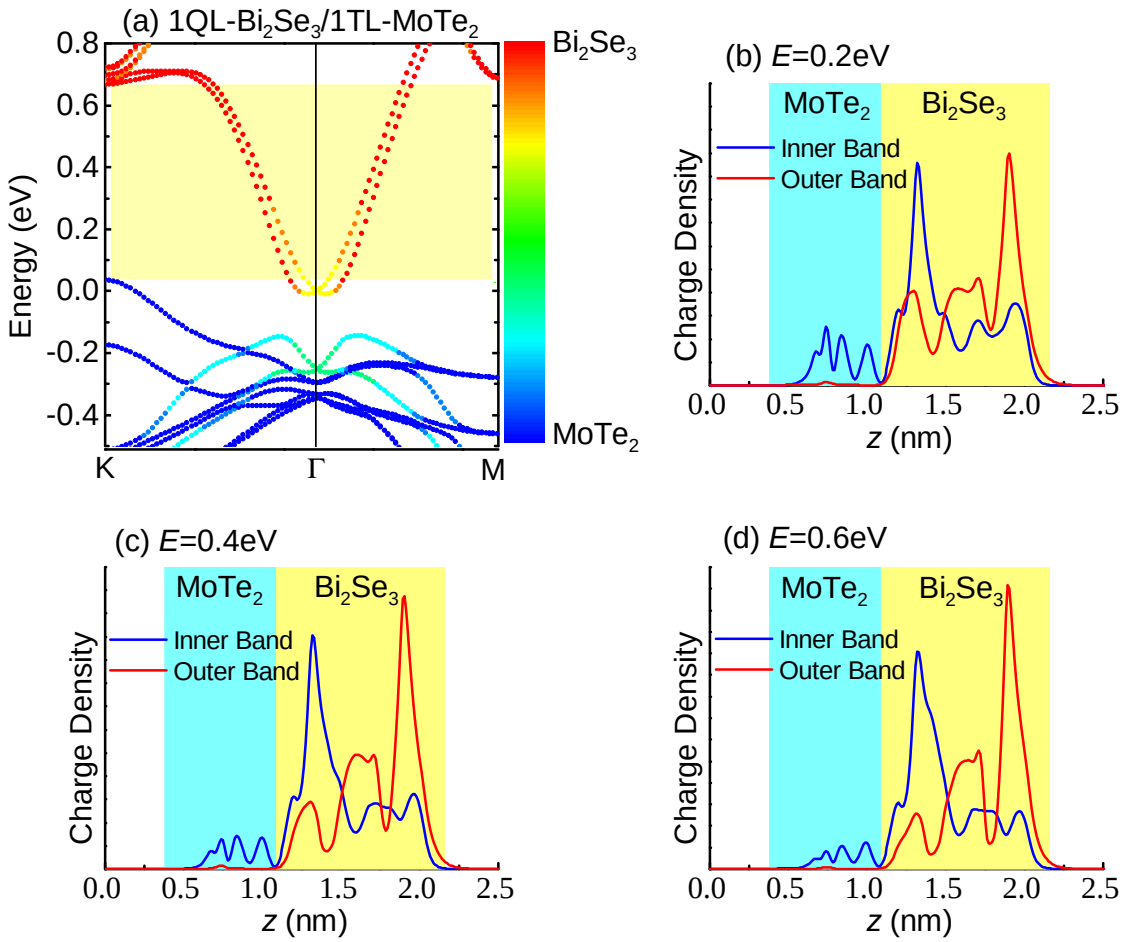

Figure S10: The electronic structure and the charge density distribution of the RB states in 1QL-Bi_2Se_3/1TL-$MoTe_2$ bilayer. (a) The band structures. (b-d) The charge density profiles of the RB states along the ΓM direction at energies 0.2, 0.4, and 0.6 eV. The cyan- and yellow-shaded regions in (b-d) indicate the $MoTe_2$ and Bi_2Se_3 layer, respectively.